

Manuscript version: Published Version

The version presented in WRAP is the published version (Version of Record).

Persistent WRAP URL:

<http://wrap.warwick.ac.uk/128813>

How to cite:

The repository item page linked to above, will contain details on accessing citation guidance from the publisher.

Copyright and reuse:

The Warwick Research Archive Portal (WRAP) makes this work by researchers of the University of Warwick available open access under the following conditions.

Copyright © and all moral rights to the version of the paper presented here belong to the individual author(s) and/or other copyright owners. To the extent reasonable and practicable the material made available in WRAP has been checked for eligibility before being made available.

Copies of full items can be used for personal research or study, educational, or not-for-profit purposes without prior permission or charge. Provided that the authors, title and full bibliographic details are credited, a hyperlink and/or URL is given for the original metadata page and the content is not changed in any way.

Publisher's statement:


Please refer to the repository item page, publisher's statement section, for further information.

For more information, please contact the WRAP Team at: wrap@warwick.ac.uk

Design of a flexure-based mechanism possessing low stiffness and constant force

Cite as: Rev. Sci. Instrum. **90**, 105005 (2019); <https://doi.org/10.1063/1.5119276>

Submitted: 10 July 2019 . Accepted: 23 September 2019 . Published Online: 21 October 2019

Yanling Tian, Chongkai Zhou, Fujun Wang , Kangkang Lu, Yanjie Yuan, Mingxuan Yang, and Dawei Zhang 



View Online



Export Citation



CrossMark

ARTICLES YOU MAY BE INTERESTED IN

[A systematic error modeling and separation method for the special cylindrical profile measurement based on 2-dimension laser displacement sensor](#)

Review of Scientific Instruments **90**, 105006 (2019); <https://doi.org/10.1063/1.5111350>

[Modeling and control methodology for an XYZ micro manipulator](#)

Review of Scientific Instruments **90**, 105007 (2019); <https://doi.org/10.1063/1.5116094>

[Measurement and control of emergent phenomena emulated by resistive-capacitive networks, using fractional-order internal model control and external adaptive control](#)

Review of Scientific Instruments **90**, 103003 (2019); <https://doi.org/10.1063/1.5097743>



Lock-in Amplifiers

Zurich Instruments

Watch the Video

Design of a flexure-based mechanism possessing low stiffness and constant force

Cite as: Rev. Sci. Instrum. 90, 105005 (2019); doi: 10.1063/1.5119276

Submitted: 10 July 2019 • Accepted: 23 September 2019 •

Published Online: 21 October 2019



Yanling Tian,^{1,2} Chongkai Zhou,¹ Fujun Wang,^{1,a)} Kangkang Lu,¹ Yanjie Yuan,¹ Mingxuan Yang,¹ and Dawei Zhang¹

AFFILIATIONS

¹Key Laboratory of Mechanism Theory and Equipment Design of Ministry of Education, School of Mechanical Engineering, Tianjin University, Tianjin 300354, China

²School of Engineering, University of Warwick, Coventry CV4 7AL, United Kingdom

^{a)}Author to whom correspondence should be addressed: wangfujun@tju.edu.cn

ABSTRACT

This paper presents a novel design of a flexure-based constant force mechanism with a long travel stroke. Unlike the conventional force control method using a force sensor and feedback controller to obtain constant force output, the proposed compliant mechanism provides a constant force utilizing the unique mechanical property of the mechanical structure. The constant force is generated by using the combination of a negative-stiffness and a positive-stiffness mechanism. In order to achieve a low driving force, the negative stiffness is realized by a special bistable beam, which is a step beam with structural holes. Meanwhile, the positive stiffness is generated by the leaf flexure hinges with structural holes. The regular structural holes can reduce the mass and stiffness of the whole mechanism. Furthermore, the elliptic integral method and the pseudo-rigid-body approach are utilized to establish the model of the constant force mechanism. Based on the established model, the performance of the constant force mechanism is evaluated computationally. Additionally, the parametric model of the proposed mechanism is investigated using the nonlinear finite element analysis. Finally, a prototype is fabricated using 3D printing technique. The open-loop and the closed-loop experimental tests are implemented to investigate the performance of the developed constant force mechanism. It is noted that the constant force mechanism can be robustly controlled by a proportional-integral-derivative control method. Experimental results demonstrate that the developed constant force mechanism has a constant force with slight fluctuation with a range of 500 μm .

Published under license by AIP Publishing. <https://doi.org/10.1063/1.5119276>

I. INTRODUCTION

With the development of micro/nanomanufacturing, the precision compliant mechanism and system have become more and more important in scanning probe microscopy,¹ micro/nanorobotics,² medical devices,³ etc. Owing to the inherent mechanical shortcomings such as friction, wear, and lubrication, it is difficult to meet the high accuracy requirement by the conventional joint based mechanisms. Thus, the flexure-based mechanisms have been widely utilized in these kinds of precision engineering.⁴⁻⁷

The constant force is usually realized by the feedback control methodology with precision force sensors and controllers. However, it needs to design the real time and complex algorithm to control the force and displacement simultaneously. The control techniques include the force/position switching control and impedance control.^{8,9} Furthermore, in order to overcome the nonlinearity of the

implicit model, the precision position control and feedback control methods are necessary for the compliant mechanism.^{10,11} In addition, for the compliant mechanism, the main deformation usually occurs at the flexible hinges. To realize high precision, the whole structure parameters should be analyzed to guarantee the limited value for deformation within the elastic domain.¹² It is more complicated to utilize the feedback control algorithm to improve the accuracy of the constant force. Because the force sensor is sensitive to the relative displacement, it is difficult to control the displacement accurately.¹³ Although the force information on the mechanism is available, the contact force between components is difficult to control accurately. Thus, the force sensor-based feedback control system needs a complicated algorithm implementation to obtain a constant contact force environment.

Recently, several zero stiffness flexure mechanisms have been proposed to obtain the constant force.¹⁴ Unlike the traditional

elastic mechanism, a new kind of constant force mechanism has been developed. The constant force mechanism does not obey Hooke's law and can realize a zero stiffness with a large displacement output, which is realized by combining a positive-stiffness mechanism and a negative-stiffness mechanism together to obtain a zero-stiffness mechanism. Thus, a constant force output is realized by the developed structure. The positive stiffness can be generated by the deformation of leaf beams, while the negative stiffness is proposed based on the buckling of prestressed bars. A vibration isolation system using the negative stiffness is designed to obtain a lower frequency.^{15,16} For these kinds of constant force mechanisms, the position control and force control are not required, which provides a good way to generate the constant force.^{17,18} Unfortunately, the constant force mechanism indicates a zero-stiffness and low resonant frequency. As a consequence, the constant force mechanism is usually utilized in static and quasistatic applications.

As a result, a novel constant force mechanism is proposed in this paper. A large motion range is realized by the mechanism with zero stiffness property. The constant force mechanism is composed by two parts: negative stiffness flexure hinges (NSFHs) and positive stiffness flexure hinges (PSFHs). Combining the NSFHs and PSFHs together, a constant force mechanism can be obtained. In particular, the structural holes are designed on the NSFHs and PSFHs, in order to reduce the mass and stiffness of the structure. Moreover, the resonant frequency of the constant force mechanism is higher than those of the traditional ones. To improve the fabrication accuracy of the mechanism, the NSFHs are designed as bistable mechanism using step beams instead of inclined flexure beams. It is much easier to fabricate the structural holes on the step beams with high precision.

The remainder of the paper is arranged as follows: the design and analytic modeling of the constant force mechanism have been introduced in Sec. II. The static and dynamic performance is analyzed using the finite element analysis (FEA) in Sec. III. Furthermore, the prototype of the system has been developed and the experiments have been conducted to validate the characteristics in Sec. IV. The conclusion is summarized in Sec. V.

II. MECHANISM DESIGN

A constant force mechanism is realized by the combination of NSFHs and PSFHs. The two parts—NSFHs and PSFHs of the designed constant force mechanism are required to be analyzed. The zero stiffness can be realized by counteracting stiffness of these two kinds of flexure hinges. In order to guarantee a long constant force stroke with low driven force, the system needs to be designed with low stiffness structure beams. Therefore, the regular structural holes are designed on the beams, which is utilized to decrease the stiffness of the combined structures. In order to determine the optimal parameters of the constant force mechanism, the analytical model is established and utilized to analyze the static characteristics.

A. Design of negative stiffness flexure hinges

For the whole constant force mechanism, the NSFHs are composed of four step leaf beams, which are connected to the support frame and the central actuating rod. To realize a large stroke with low driving force, the structural holes are designed on the beams, as shown in Fig. 1. The traditional negative stiffness flexure hinges are realized by an inclined bistable beam. However, it is more convenient and accurate to fabricate the structural holes on the horizontal leaf flexures, comparing to the inclined leaf beams. Thus, a novel step beam with the good static and dynamic characteristics is proposed, as shown in Fig. 2. When the NSFH is designed with step beams, it can be considered as an inclined angle beams. A large bending deformation of the beam will lead to a buckle effect. Furthermore, to decrease the stiffness and mass of NSFHs, the structural holes are fabricated regularly. The step beams can be considered as a bistable beam. When the beams bend with a large deformation, the bistable behavior will occur during the deformation progress.

To obtain a reliable performance of the NSFH, the theoretical model is established and analyzed. Recently, many methods have been proposed to evaluate the characteristics of the bistable beams, such as the elliptic integral model,¹⁹ finite element model,²⁰ and pseudo-rigid-body model.²¹ There are some advantages for the step beams, acting as bistable beams, instead of the inclined beams.

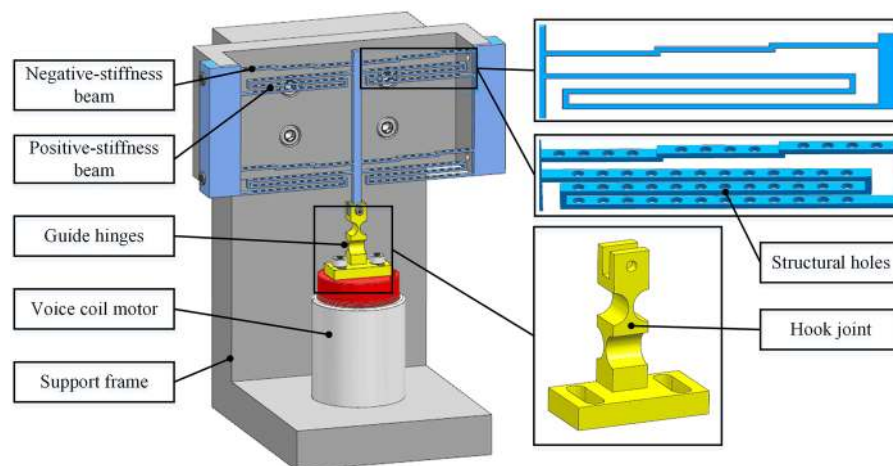


FIG. 1. Overall structure of the proposed constant force system.

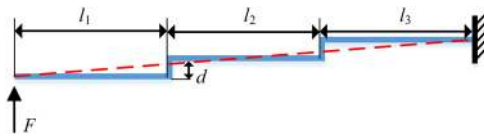


FIG. 2. The structure of step leaf hinge.

For example, it is very convenient to fabricate the regular structural holes, owing to the step beams designed in horizontal. Furthermore, the step beam has the same bistable characteristics as an inclined beam during the bending process. In addition, the performance of the NSFH is nonlinear, so the elliptic integral method is utilized to determine the parameters. Then, the finite element analysis method is used to study the structure characteristics.

The Bernoulli-Euler equation is used to investigate the performance of bistable beams, which is an important part of the elliptic integral method. The relationship between force, angle, and bending deformation is shown in Fig. 3. The deviation of the formula is defined as follows:

$$EI \frac{d(\theta)}{ds} = M - F \cdot x_a \cdot \sin \alpha + F \cdot y_a \cdot \cos \alpha. \quad (1)$$

In order to solve the Bernoulli-Euler equation, the following equations are used, which can eliminate the variables x_a and y_b :

$$\frac{d\theta}{ds} = \frac{d\theta}{dx_a} \frac{dx_a}{ds} = \frac{d\theta}{dx_a} \cdot \cos \theta, \quad (2)$$

$$\frac{d\theta}{ds} = \frac{d\theta}{dy_a} \frac{dy_a}{ds} = \frac{d\theta}{dy_a} \cdot \sin \theta. \quad (3)$$

Differentiating Eq. (1) with respect to s and combining Eqs. (2) and (3), the following equation is obtained:

$$EI \frac{d^2\theta}{ds^2} = F \cdot \cos \theta + F \cdot \sin \theta. \quad (4)$$

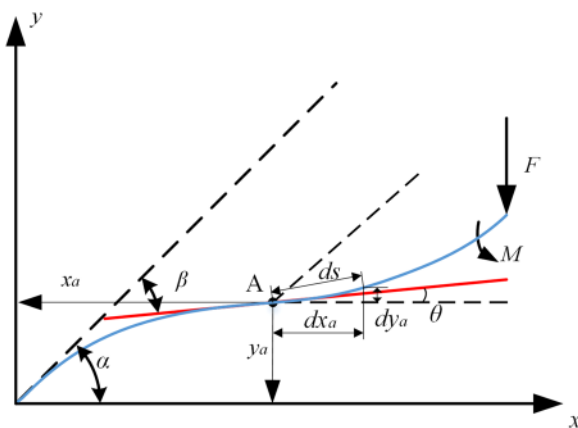


FIG. 3. Schematic diagram of a bistable beam with parameter.

Integrating Eq. (4) with respect to θ yields

$$EI \left[\frac{d\theta}{ds} \right]^2 = F \cdot \sin \theta - F \cdot \cos \theta + C. \quad (5)$$

The position of point A can be determined by the following equations:

$$y_a = \sin \theta ds, \quad (6)$$

$$x_a = \cos \theta ds. \quad (7)$$

The first elliptic integral equation is used to analyze the model. Two parameters are defined as γ and λ ,

$$\cos \frac{2\alpha - \beta}{2} = \lambda \sin \gamma. \quad (8)$$

A new parameter N is defined as the reaction force, which can be calculated by

$$N = F(\lambda, \gamma_1) - F(\lambda, \gamma_2). \quad (9)$$

The whole analytical models can be derived as follows:

$$\frac{x_a}{L} = -\frac{1}{R} \{ 2 \cos \beta [E(\gamma, \beta_1) - E(\gamma, \beta_2) - F(\gamma, \beta_2) + F(\gamma, \beta_1)] + 2\gamma \cos \alpha (\cos \beta_2 - \cos \beta_1) \}, \quad (10)$$

$$\frac{y_a}{L} = -\frac{1}{R} \{ 2 \sin \beta [E(\gamma, \beta_2) - E(\gamma, \beta_1) - F(\gamma, \beta_2) + F(\gamma, \beta_1)] + 2\gamma \cos \alpha (\cos \beta_1 - \cos \beta_2) \}, \quad (11)$$

where

- E is the the Young's modulus,
- I the rotational inertia of the beam,
- x_a the X coordinate of point A,
- y_a the Y coordinate of point A,
- α the inclined angle of the beam,
- β the angle of gradient line of point A,
- L the length of the beam,
- F the force and moment of the bistable beam,
- M the moment of the bistable beam, and
- C a constant value.

$E(\gamma, \beta)$ and $F(\gamma, \beta)$ are the first-kind and second-kind elliptic integral, respectively.²² By utilizing the analysis model, the relationship between the reaction force and displacement can be obtained. The main parameters of the constant force mechanism are given in Table I.

For the theoretical analysis, the main parameters L_1, L_2, L_3 of the PFSH are the lengths of flexure hinges. D is the displacement

TABLE I. Parameters of the constant force mechanism.

Parameters (PSFH)	L_1	L_2	L_3	D	W	T
Values (mm)	55	50	55	2	3	1
Parameters (NSFH)	l_1	l_2	l_3	d	w	t
Values (mm)	19	20	19	0.8	3	1

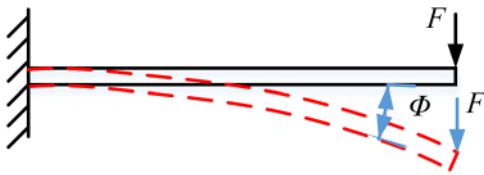


FIG. 4. Schematic diagram of a traditional leaf beam.

of two closed flexure beams, while W and T are the width and thickness. Besides, l_1, l_2, l_3 are the length of each step beam hinges, respectively. d is the displacement of two flexure hinges, and w, t are the width and thickness of NFSH, respectively.

The PSFHs are usually designed as the slender leaf beam, owing to the advantages of stable characteristic performance and easy to fabricate. However, a lower stiffness flexure beam has a longer physical size. Owing to the limit capacity of current machining fabrication, it is difficult to decrease the thickness of beams with high accuracy. Thus, the size of whole mechanism is normally quite large. It usually uses a long rather than a thin leaf flexure. In addition, the long slender leaf flexure changes to be stress stiffening during the motion of the mechanism. Furthermore, the transverse stiffness increases owing to the stress stiffening, as shown in Fig. 4.

The structural holes are evenly distributed on the beams. The diameter of each holes is 2 mm and the center to center separation between two adjacent holes is 4 mm. Owing to the traditional leaf beam, it is convenient to fabricate the structural holes. In addition, better constant force characteristics is obtained with a reliable stroke by combining the NSFHS and the PSFHs.

B. The design of positive stiffness flexure hinges (PSFHs)

The slender leaf flexure beam is usually chosen for the positive-stiffness structure. However, from the machinability point of view, a long leaf flexure beam is commonly utilized to decrease the stiffness of the flexures, leading to a large size of the stage. Consequently, the dynamic performance of the stage is influenced. The resonance frequency of the mechanism is usually low. The stress stiffening phenomenon also occurs during the motion of the stage, which leads to the dramatically increasing of the stiffness. Along with the increase of the tensile stress, the stiffness of the flexure will increase dramatically. Nevertheless, the higher the compressive stress, the lower stiffness of the flexure. In order to overcome the disadvantages mentioned above. A novel shape of leaf flexure is designed as the PSFH in this work, as shown in Fig. 5. The N shape flexure is applied in the PSFHs. When an input force loads on the flexure, each of leaf flexures suffers from a combined force and generates a bending deformation, correspondingly. Furthermore, the stress stiffening is avoided by the novel structure PSFHs. Based on the characteristics of mechanics of materials, the stiffness of the PSFH is derived as

$$\frac{Fl^2}{2EI} - \frac{Ml}{EI} = 0, \quad (12)$$

$$\frac{Fl^3}{3EI} - \frac{Ml^2}{2EI} = \delta_x. \quad (13)$$

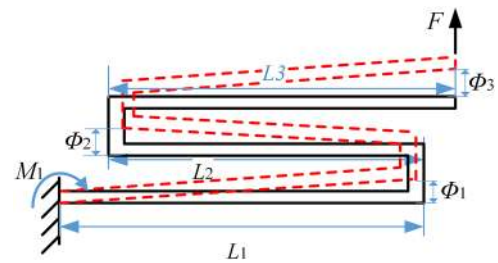


FIG. 5. Schematic diagram of PSFHs.

According to Eqs. (12) and (13), the displacement δ_x can be calculated as

$$\delta_x = \frac{Fl^3}{12EI}. \quad (14)$$

The stiffness of the PSFH is defined as follows:

$$k = \frac{F}{\delta_x} = \frac{Ebt^3}{nl^3}, \quad (15)$$

where

- l is the length of the flexure,
- b the width of the flexure,
- t the thickness of the flexure, and
- n the number of the flexure.

C. Kinematic analysis of the constant force mechanism

The flexure hinges in the constant force mechanism are composed of NSFHS and PSFHs. The relationship between the reaction force F is described as

$$F = F_P + F_N. \quad (16)$$

According to pseudo-rigid-body model (PRBM), the input force can be described as following:

$$F_P = \sum_1^3 F_{\Phi_i}. \quad (17)$$

It can be expressed as

$$F_{\Phi_i} = \frac{2EI\Phi_i}{L_i^2}. \quad (18)$$

As shown in Fig. 5, E and I represent the Young's modulus and the second moment of area. Furthermore, the angle Φ_i can be calculated by

$$L_1 \sin \Phi_1 + L_2 \sin \Phi_2 + L_3 \sin \Phi_3 = \delta, \quad (19)$$

where

- F_P is the reaction force of the PSFH along x axis,
- F_N the reaction force of the NSFH along x axis,
- F_{Φ_i} the loading force of the PSFHs along x axis,
- Φ_i the changing angle, and
- δ the total displacement of the system.

Both of the NSFHs and the PSFHs have structural holes, the total stiffness of the constant force mechanism is calculated by the simulation.

III. COMPUTATIONAL ANALYSIS OF SYSTEM COMPONENT

In the section, a novel constant force system is designed and the finite element analysis (FEA) is utilized to analyze the static characteristics. The static models of the NSFH, the PSFH, and the combined structure are extensively investigated to obtain insights into the performance of the developed mechanisms.

A. Static characteristics analysis

The whole system is composed of a pair of combination structures. The performance of the designed mechanism with the NSFHs and the PSFHs is analyzed by the ANSYS Workbench software, which is suitable for analyzing the nonlinear relationship between force and displacement. Hence, the performances of the NSFHs and the PSFHs are analyzed by the software. Furthermore, in order to get a low stiffness beams, the structural holes are designed on the NSFHs and the PSFHs. A static structure analysis is carried out to evaluate the property of the beams.

The polylactic acid (PLA) is chosen as the material of the constant force mechanism. The PLA has a value of 3000 MPa elasticity modulus and owns a relatively high elastic property. Furthermore, the density of the material is 1200 kg/m^3 , which helps to reduce the mass of the whole system. As shown in Fig. 6, the whole structure is installed to the support frame. A driving force $1000 \mu\text{N}$ is loaded on the end of the moving rod. The corresponding displacement of the moving rod is $6.30 \mu\text{m}$. The experimental studies will be conducted to study the actual properties of the fabricated prototype. And the influence of different materials will be investigated in the future work.

In order to analyze the characteristics of the NSFH and PSFH, the simulations are implemented, respectively. The positioning holes are fixed and a driving force $1000 \mu\text{N}$ is applied on the other end. The simulation result shows that the maximum stress is 0.025 MPa, which is much lower than the tensile strength 125 MPa of the material PLA. Therefore, the material can be utilized to fabricate the structure with good performance.

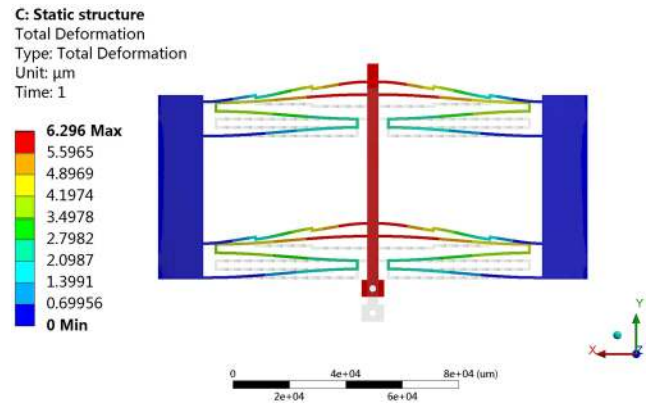


FIG. 6. Simulation study of the whole system.

The simulation results of the NSFH, the PSFH, and the combined structure are provided in Figs. 7–9, respectively. These figures show the different performance of the components with or without structural holes. The stiffness of the NSFH, the PSFH, and the combined structure with holes are 2.06 N/m, 0.76 N/m, and 7.82 N/m, respectively, whereas the structures without holes have higher stiffness, which are 3.62 N/m, 1.34 N/m, and 14.1 N/m, respectively. Furthermore, the corresponding ratios of the stiffness between structures are 0.57, 0.57, and 0.55, respectively. The parameters are summarized in Table II.

With a driven force $1000 \mu\text{N}$ on the moving rod, the deformations of the whole structures with and without structural holes are shown in Figs. 10(a) and 10(b), respectively. As the figures show, the stiffness of the structures with and without holes are calculated as 7.82 N/m and 14.1 N/m, respectively.

According to the simulation results, both the NSFHs and the PSFHs with structural holes have lower stiffness than the ones without holes, as shown in Table II. The stiffness of different structures obviously decreased with the structural holes. As the designed constant force mechanism, the stiffness is changing with the deformation of the flexure beams. In the constant travel, the stiffness is decreasing close to zero and the frequency is close to zero.

For the designed structure with holes, there are 12 structural holes on each NSFH, with the diameters of 2 mm. The separation

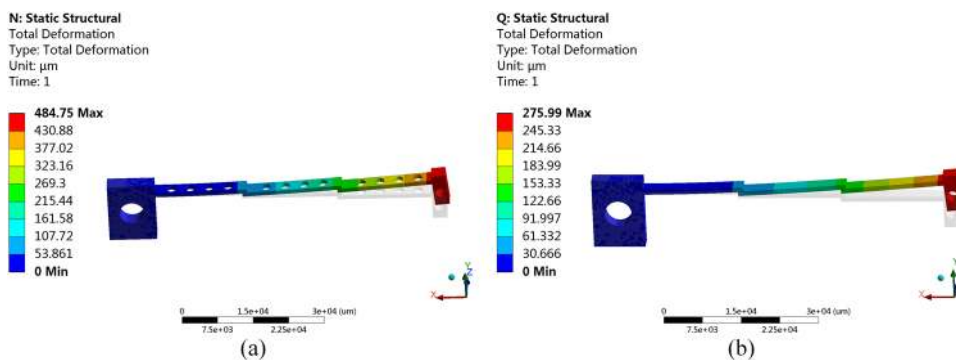


FIG. 7. Simulation study of the NSFH: (a) with structural holes, (b) without structural holes.

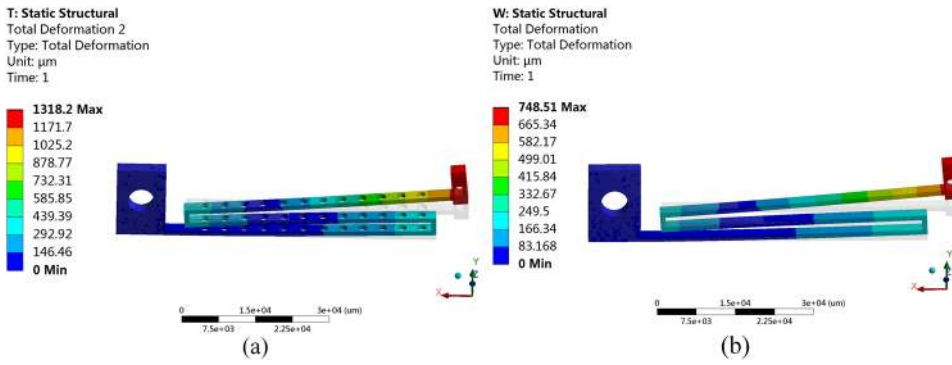


FIG. 8. Simulation analysis of the PSFH: (a) with structural holes, (b) without structural holes.

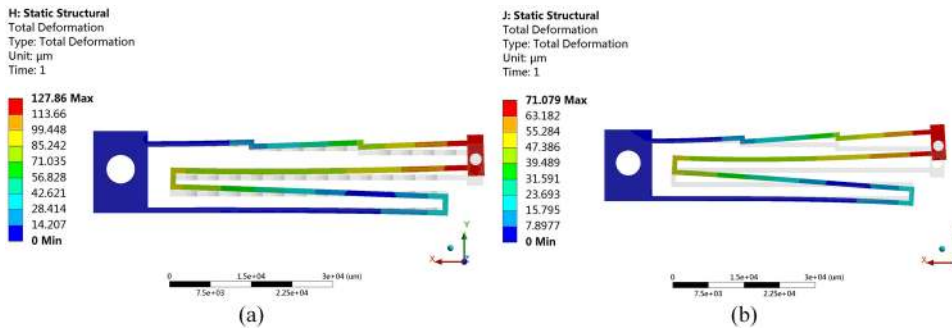


FIG. 9. Simulation of combined the NSFH and the PSFH: (a) with structural holes, (b) without structure holes.

distance of every two structural holes is 4 mm. Every PSFH is composed of three leaf flexure hinges. During the simulation, the whole structure is fixed by the poisoning holes and an increasing force is loaded on the moving rod. The relationship between the interaction force and the displacement is shown in Fig. 11. The constant force is occurred at 10 mN with a range of 550 μm.

B. Modeling analysis of the mechanism

The dynamics of the constant force mechanism is examined by ANSYS Workbench software. The simulation results of the model shapes are shown in Fig. 12. The first three resonant frequencies of the constant force mechanism are 39.4 Hz, 44.3 Hz, and 44.6 Hz,

TABLE II. Simulation results of the structure hinges.

Parameters	Stiffness (N/m)			First response frequency (Hz)		
	NSFH	PSFH	Combined	NSFH	PSFH	Combined
With holes	2.06	0.76	7.82	25.7	14.9	31.4
Without holes	3.62	1.34	14.1	32.5	18.74	36.8
Ratio	0.57	0.57	0.55	0.79	0.79	0.85

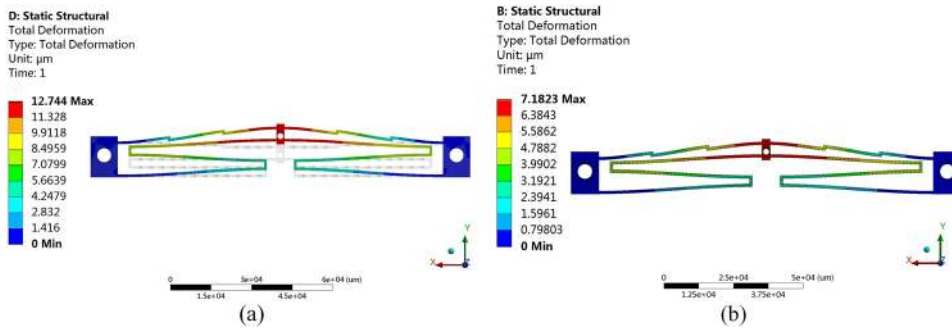


FIG. 10. Simulation of combined the NSFH and the PSFH: (a) with structural holes, (b) without structural holes.

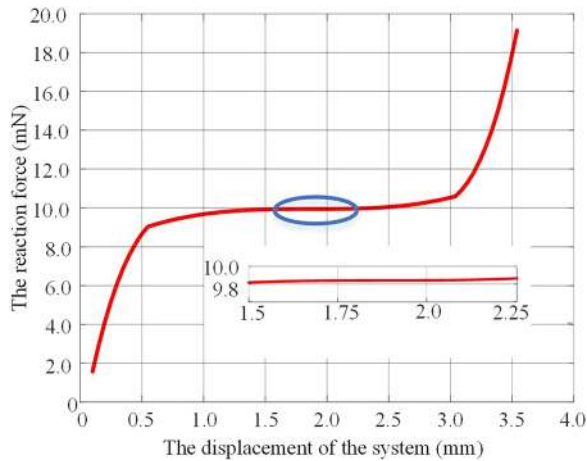


FIG. 11. Simulation result of force-displacement relationship for the constant force mechanism.

respectively. In addition, it is obvious the translational movement along y axis as the first resonant mode. The structural holes on the beams have less influence to the frequencies. Hence, the novel constant force mechanism has low stiffness with relatively high resonant frequency. The designed constant force mechanism is suitable for manipulation with the low magnitude force. In practical operation, the current frequency of experiment is usually lower than 10 Hz. Hence, the resonant frequency is high enough for the applications.

IV. EXPERIMENTAL TESTS

In the section, the prototype has been developed and shown in Fig. 13. A series of experimental tests have been conducted to verify the performance of the constant force mechanism. The step beams can realize bistable beam performance. Besides, the structural holes on the beams lead to low stiffness and reduce the mass of the structure with a relative stable dynamic performance. During fabrication progress, the accuracy of NSFH with structural holes is easy to be guaranteed, owing to the horizontal step beam structure.

A. Prototype fabrication

The 3D printing technique is utilized to fabricate the prototype of the constant force mechanism, as depicted in Fig. 13. The material of the structure is PLA, which is one of the commonly used materials in 3D printer. Considering the force and stroke requirements, a voice coil motor is selected for the actuation. The voice coil motor (model: NCC05-18-060-2X, H2W) is driven by a commercial linear servo amplifier (model: LCAM5/15, H2W) to deliver a nominal travel stroke of 12.7 mm. In order to measure the displacement of the constant force mechanism, a laser displacement sensor (model: LK-H050, KEYENCE CORPORATION) is utilized. A force sensor load cell (F329, Novatech Measurements Limited) with a range of 100 mN and a resolution of $4 \mu\text{N}$ is chosen to measure the reaction force. Furthermore, a control board (model: DS 1103 R&D, DSPACE) is utilized to realize a real-time control for the constant force mechanism. The control algorithms are programmed by MATLAB/Simulink software to realize a deterministic control for the constant mechanism. The overall system is installed on a Newport optical table for the reduction of external disturbances from the environment.

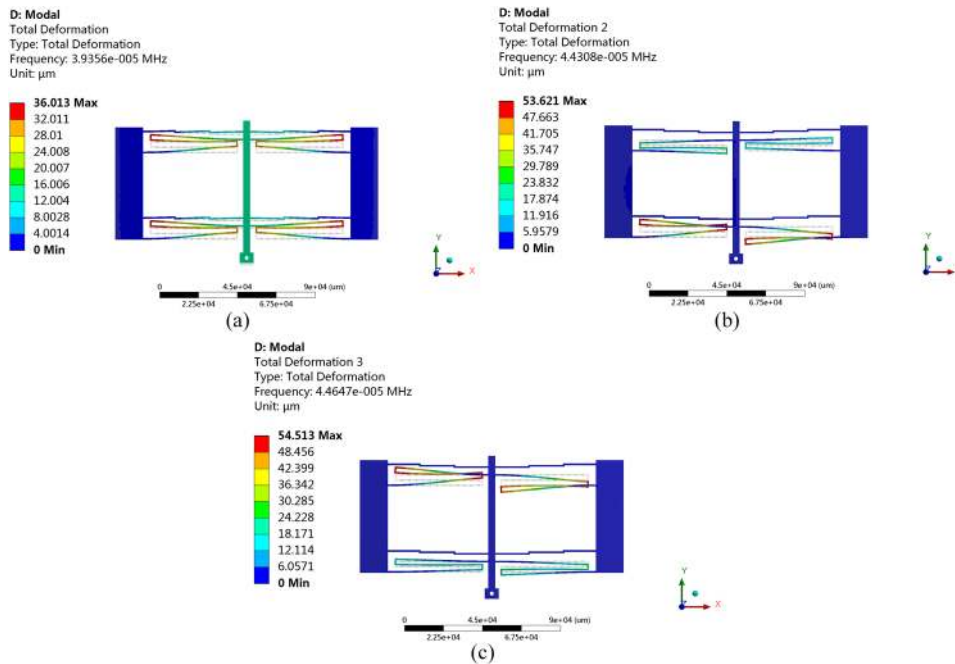


FIG. 12. Resonant frequencies and mode shapes of the constant force mechanism: (a) First mode. (b) Second mode. (c) Third mode.

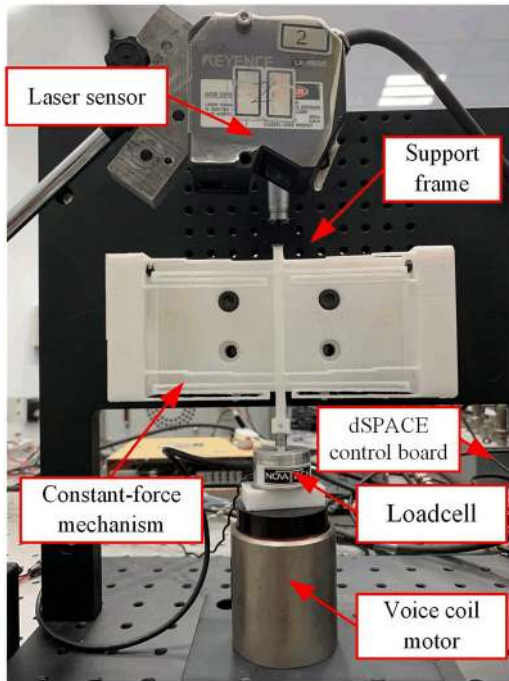


FIG. 13. Experimental setup of the constant force system.

B. Relationship test between force and displacement

The open-loop and close-loop control experiments are implemented to investigate the performance of the mechanism.

For the open-loop control test, as shown in Fig. 13, the displacement laser is used to measure the position of the system with an increasing current to the voice coil motor. It is observed that the proposed structure has a constant force travel of 500 μm, as shown in Fig. 14. The curve increases suddenly when the system turns to relative zero stiffness.

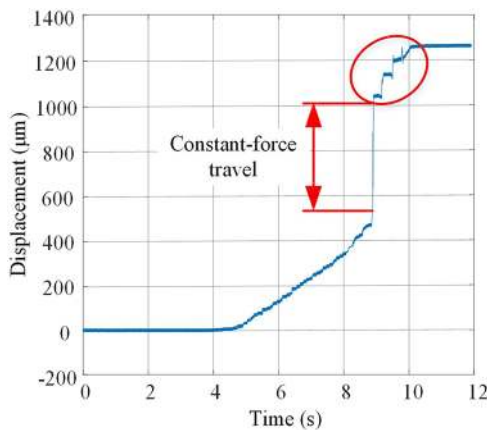


FIG. 14. The force-displacement relationship of the constant force mechanism by open-loop control experiment.

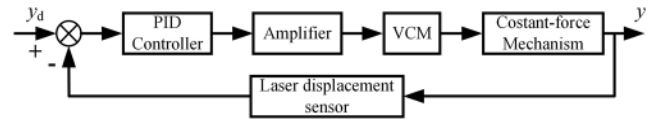


FIG. 15. Block diagram of feedback controller.

In order to improve the stability and repeatability, a proportional-integral-derivative (PID) controller is utilized to compensate the displacement of the system. The block diagram of feedback controller is shown in Fig. 15. The output displacement y is measured by the laser sensor and the position error can be calculated by the desired value y_d and the output value. The controlled model is established by Matlab/Simulink and realized by the dSPACE control board. The PID controller is defined as follows:

$$y_d = K_p e_d(t) + K_I \int_0^t e_d(t) dt + K_D \frac{de_d(t)}{dt}, \quad (20)$$

where K_p , K_I , and K_D represent the proportional gain, integral gain, and differential gain, respectively. According to the Ziegler-Nichols method, the parameters of PID controller are $K_p = 0.001$, $K_I = 0.0001$, and $K_D = 0$.

The closed-loop control method is utilized with the PID algorithm. A stable increasing force acts on the structure. Meanwhile, the laser displacement sensor measures the changing position, as shown in Fig. 16. A constant force of 10.04 mN keeps a stroke of 500 μm with a resolution of 25 μm.

Owing to the combined the NSFHs and the PSFHs, the constant force mechanism realizes a zero stiffness with a respect travel. The experimental results show a constant force travel of 500 μm.

According to the results between simulation analysis and experimental test, the reaction forces illustrate the accuracy of the established models. Unlike the traditional beams, it is observed that the reaction force of the proposed structure cannot be adjusted an arbitrary value. Because the reaction force is determined by the constant force beams, the ways of changing the force includes redesigning the parameters of the beams and so on. The most influential factor for the discrepancy is the fabrication capacity of the 3D printing. Therefore, the trend of the constant force may differ between the simulated and experimental results, as shown in Figs. 11 and 16. However,

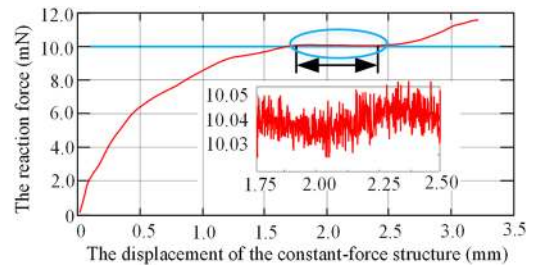


FIG. 16. The force-displacement relationship of the constant force mechanism by closed-loop control experiment.

the value of the constant force are approximately the same. In addition, the accuracy of laser displacement sensor is another important deviation factor.

V. FURTHER DISCUSSION

The advantages of the developed constant force mechanism have been exhibited by the experiments. In addition, it is an easy way to realize a constant force control by the position control instead of considering the force controller. On the other hand, the proposed constant force mechanism has been applied in various aspects. The smart cutting tool can be implied the constant force mechanism, which can not only compact the whole system size, and also enhance the cutting tool life by the desired force range.^{23,24} Moreover, the future work may be conducted to design a constant force mechanism with the adjustable reaction force.

VI. CONCLUSIONS

This paper presents a novel flexure-based constant force mechanism with long travel and low stiffness. The constant force mechanism is composed of the NSFHs and the PSFHs. For the NSFHs, the step beams are utilized with structural holes. Besides, the PSFHs are designed as Z shape leaf flexure hinges with structural holes. The analytical model was established to analyze the characteristics of the mechanism. Furthermore, the performance of the constant force mechanism has been derived and verified by the FEA simulation. The regular structural holes decrease the stiffness of the whole mechanism. Nevertheless, the mechanism keeps the relative high resonant frequency. Moreover, the prototype mechanism is fabricated by a 3D printer and a series of experiments are implemented. The open-loop and closed-loop experiments have been implemented. The experimental results indicated that the proposed mechanism could realize a travel of 500 μm under a driving force 10.04 mN. The PID controller is utilized to robustly control to the system. The constant output force exhibits a fluctuation of less than 25 μN , which reveals a good motion repeatability.

ACKNOWLEDGMENTS

This research is supported by the National Natural Science Foundation of China (Grant Nos. 51675371, 51675367, and 51675376), the National Key R&D Program of China (Grant Nos. 2016YFE0112100, 2017YFB1104700, and 2017YFE0112100), the Science and Technology Commission of Tianjin Municipality

(Grant Nos. 19PTZWHZ00010 and 18PTZWHZ00160), and the EU H2020 Program MNR4SCell (Grant No. 734174).

REFERENCES

- ¹K. Cai, Y. Tian, F. Wang, D. Zhang, X. Liu, and B. Shirinzadeh, *Rob. Comput. Integr. Manuf.* **44**, 77 (2017).
- ²C. Werner, P. C. J. N. Rosielle, and M. Steinbuch, *Int. J. Mach. Tools Manuf.* **50**, 183 (2010).
- ³G. Wang and Q. Xu, *IEEE/ASME Trans. Mechatronics* **22**, 1744 (2017).
- ⁴L. L. Howell, *Encycl. Nanotechnol.* **10**, 604 (2001).
- ⁵Q. Xu, *Rev. Sci. Instrum.* **85**, 025002 (2014).
- ⁶Y. Qin, B. Shirinzadeh, Y. Tian, D. Zhang, and U. Bhagat, *IEEE/ASME Trans. Mechatronics* **19**, 872 (2013).
- ⁷Y. Yuan, D. Zhang, X. Jing, H. Zhu, W.-L. Zhu, J. Cao, and K. F. Ehmann, *Int. J. Mech. Sci.* **152**, 454 (2019).
- ⁸H. Huang, D. Sun, H. Su, and J. K. Mills, *Adv. Rob. Virtual Reality* **26**, 61 (2012).
- ⁹Y. K. Yong, A. J. Fleming, and S. Moheimani, *IEEE/ASME Trans. Mechatronics* **18**, 1113 (2012).
- ¹⁰L. J. Lai, G. Y. Gu, and L. M. Zhu, *Rev. Sci. Instrum.* **83**, 045105 (2012).
- ¹¹Z. Guo, Y. Tian, C. Liu, F. Wang, X. Liu, B. Shirinzadeh, and D. Zhang, *Rob. Comput.-Integr. Manuf.* **32**, 93 (2015).
- ¹²S. P. Wadikhaye, Y. K. Yong, and S. Reza Moheimani, *Rev. Sci. Instrum.* **85**, 105104 (2014).
- ¹³Q. Xu, *IEEE Trans. Automation Sci. Eng.* **14**, 1 (2015).
- ¹⁴A. J. Lamers, J. A. G. Sánchez, and J. L. Herder, *Mech. Mach. Theory* **92**, 230 (2015).
- ¹⁵D. L. Platus, in *Proceedings of Vibration Control in Microelectronics, Optics, and Metrology* (International Society for Optics and Photonics, 1992).
- ¹⁶F. Liu, X. Pang, Z. Liu, T. Zhang, H. Huang, and J. Zhu, in *Proceeding of the 3rd International Nanoelectronics Conference*, Hong Kong, 2010.
- ¹⁷F. M. Morsch and J. L. Herder, in *Proceedings of ASME 2010 International Design Engineering Technical Conferences and Computers and Information in Engineering Conference* (American Society of Mechanical Engineers, 2010).
- ¹⁸H. T. Pham and D. A. Wang, *Mech. Mach. Theory* **46**, 899 (2011).
- ¹⁹B. Todd, B. D. Jensen, S. M. Schultz, and A. R. Hawkins, *J. Mech. Des.* **132**, 071011 (2010).
- ²⁰B. J. Hansen, C. J. Carron, B. Jensen, A. Hawkins, and S. Schultz, *Smart Mater. Struct.* **16**, 1967 (2007).
- ²¹P. Soroushian, H. Chowdhury, and A. Nossoni, *J. Intell. Mater. Syst. Struct.* **14**, 475 (2003).
- ²²P. Wang and Q. Xu, in *Proceedings of IECON 2016-42nd Annual Conference of the IEEE Industrial Electronics Society* (IEEE, 2016).
- ²³C. Wang, S. B. Ghani, K. Cheng, and R. Rakowski, *Proc. Inst. Mech. Eng., Part B* **227**, 249 (2013).
- ²⁴K. Cheng and D. Huo, *Micro-Cutting: Fundamentals and Applications* (John Wiley & Sons, 2013).